Optics Letters

Dynamic polarization flip in nanoripples on photoexcited Ti surface near its surface plasmon resonance

S. I. Kudryashov,[1,2,*] S. V. Makarov,[2] A. A. Ionin,[2] C. S. R. Nathala,[3,4] A. Ajami,[3,5] T. Ganz,[4] A. Assion,[4] and W. Husinsky[3]

[1]ITMO University, Kronverkskiy Prospect 49, St. Petersburg 197101, Russia
[2]Lebedev Physical Institute, Leninsky Prospect 53, Moscow 119991, Russia
[3]Institute of Applied Physics, Vienna University of Technology, Wiedner Hauptstrasse 8-10, 1040 Vienna, Austria
[4]Femtolasers Productions GmbH, Fernkorngasse 10, 1100 Vienna, Austria
[5]Faculty of Physics, Semnan University, Semnan, Iran
*Corresponding author: sikudr@sci.lebedev.ru

Received 23 September 2015; accepted 30 September 2015; posted 1 October 2015 (Doc. ID 250310); published 22 October 2015

Both normal and abnormal sub-100-nanometer ripples (wavenumber ~10 μm^{-1}) were separately observed on Ti surfaces excited by linearly polarized IR femtosecond laser pulses at lower and higher fluences. Numerical modeling of dispersion curves for surface plasmon–polaritons on the photoexcited Ti surfaces demonstrates its surface plasmon resonance with the peak wavenumber ~8 μm^{-1} spectrally tuned by prompt surface optical response, prompt surface charging, and pre-oxidation, with normal/abnormal nanoripples appearing at its red/blue shoulders, respectively.

OCIS codes: (320.0320) Ultrafast optics; (240.6680) Surface plasmons; (140.3390) Laser materials processing; (220.4241) Nanostructure fabrication.

http://dx.doi.org/10.1364/OL.40.004967

Artificial anisotropic nanostructured metamaterials with epsilon-near-zero (ENZ) optical characteristics have been the subject of intense advanced studies during recent years [1–6]. Such metamaterials demonstrate cloaking [1,2], polarization switching [3], total transmission, and reflection [1], as well as sub-wavelength flux control effects [1,4–6], resulting from their optical anisotropy with one ENZ component [1] (see the bibliography in [1–4]).

Dynamic ENZ effect can be observed in optically tunable materials with strong interband transitions, exhibiting semiconductor-like character in the optical range [7]. For example, ultrafast optics of Ti surfaces strongly photoexcited by near-IR femtosecond laser pulses, demonstrates prompt fluence-dependent bleaching of interband transitions from high-density d-states in the valence band to low-density s-states in the conduction band and simultaneous rise of intraband transitions, both non-monotonously modulating the material dielectric function at the laser wavelength [8], as compared to simple metals such as Al [9]. As a result, its surface plasmon resonance (SPR) can be potentially blueshifted from the IR spectral range owing to the laser-increased s-band electron density ρ, or redshifted from the UV as a result of the laser-bleached d-band electron density [8,10]. However, so far, only near-wavelength ripples and their higher harmonics were observed for such tunable materials [11–17] with almost no indications of excited SPR, imprinted in surface nanoscale laser-induced periodical surface structures (LIPSS)—nanoripples [7]. Meanwhile, mysterious nanoripples with sub-100-nanometer periods, appearing as normal and/or abnormal surface nanogratings with their ridges perpendicular or parallel to laser polarization [8,18–21], have not yet been explained. Formally, according to the common dispersion relationship for surface plasmon-polaritons [22],

$$K_{\mathrm{SPP}} = \Re e\left(\frac{1}{\lambda}\sqrt{\frac{\varepsilon_m \varepsilon_d}{\varepsilon_m + \varepsilon_d}}\right), \quad (1)$$

such short ripple periods can be achieved via excitation of counterpropagating ultimately short-wavelength surface plasmons at $|\Re e(\varepsilon_m)|$ tending to $\Re e(\varepsilon_d)$, where $\Re e(\varepsilon_m) < 0$ and $\Re e(\varepsilon_d) > 0$ for the dielectric functions of the SPP-carrying conducting medium and its adjacent isolating medium, ε_m and ε_d, respectively, and their mutual interference, resulting in a standing surface EM pattern with periodicity of $1/(2K_\infty)$. Exactly at SPR one has $\Re e(\varepsilon_m) = -\Re e(\varepsilon_d)$, making its peak wavenumber K_∞ and width dependent only on $\Im \mathrm{m}(\varepsilon_m)$, while calculations of K_∞ go beyond the common approximation $\Re e(\varepsilon_m) \ll -\Re e(\varepsilon_d)$, $|\Re e(\varepsilon_m)| \gg \Im \mathrm{m}(\varepsilon_m)$ with its simple expression for $K_{\mathrm{SPP}} \approx \Re e(\frac{1}{\lambda}\sqrt{\varepsilon_d})$ [22].

In this Letter, we report on experimental observation of the dynamic polarization flip-off for surface nanoripples on Ti surfaces, photoexcited by linearly polarized ultrashort laser pulses. Their different polarizations appear on different shoulders of the surface plasmon resonance of the photoexcited Ti surface, which is tuned, along with its prompt dielectric function and prompt surface charging, through variation of fs-laser fluence, as shown by modeling its electromagnetic dispersion curves.

0146-9592/15/214967-04$15/0$15.00

Laser nanostructuring of Ti surfaces was performed in a scanning mode by 744 nm, 100 fs Ti:sapphire laser pulses with a pulse energy of 0.3 mJ, which were focused onto an optically polished bulk Ti samples by an uncoated silica lens (the focal length $f = 80$ mm) into a focal spot of 1.1 mm in 1/e-diameter, yielding the peak fluence $F = 29$ mJ/cm^2. The sample was arranged on a motorized translation stage and moved at a speed of 6 μm/s, providing the sample exposure with $N = 1.5 \times 10^3$ pulses/spot at a 10 Hz repetition rate.

At the 744 nm laser wavelength and fluence $F \approx 29$ mJ/cm^2, normal coarse ripples (low-spatial-frequency LIPSS, LSFLs) with orientation of ridges, perpendicular to the laser polarization, and spatial periods $\Lambda_L(744\text{ nm}) \approx 0.42$ μm [Fig. 1(a)], were produced in this Letter on the optical quality surface of the bulk Ti sample under near-threshold cumulative exposure ($N = 1.5 \times 10^3$) when surface ripples appear inhomogeneously, predominantly around some nano/microscale scratches, pits, or contaminants. Besides LSFLs, much finer normal second-harmonic (SH) ripples with $\Lambda_{2L}(744\text{ nm}) \approx 0.18$ μm were also observed [Fig. 1(b)]. Both LSFL and SH LSFL ripples were usually surrounded by ultrafine ripples with the same normal orientation (normally-aligned high-spatial-frequency LIPSS, n-HSFL) and a period $\Lambda_{nH}(744\text{ nm}) \approx 0.06$–$0.08$ μm [Fig. 1(a)–1(d)].

Moreover, other multi-shot nanoripples with the abnormal (abnormal HSFLs, a-HSFL) orientation and similar periods $\Lambda_{aH}(744\text{ nm}) \approx 0.07$ μm were homogeneously observed everywhere across the central part of the focal spot [Fig. 1(a)–1(d)], in agreement with our previous experimental findings for other fs-laser wavelength, pulse widths, and Ti samples [21].

Hence, both abnormal (homogeneous) and normal (heterogeneous, e.g., scratch-induced) types of HSFL nanoripples were observed on these Ti surfaces, excited by the linearly polarized IR fs-laser pulses, in the narrow laser fluence range around ≈30 mJ/cm^2 (see also [19,21]), as compared with the broad fluence range of ≈80–350 mJ/cm^2 for LSFL persistence [19]. This indicates a rather narrow fluence range, in which these structures are produced, and may be ascribed to IR fs-laser excitation of spectrally narrow and fluence-tunable SPR on Ti surfaces. The observation of second-harmonic normal ripples strongly supports this point, since at the fixed laser wavelength large SPP wavenumbers K_{SPP} can be achieved only in the SPR proximity, as illustrated below in Fig. 3. The observed swelling of the materials along the nanoripple ridges for incident fs-laser fluences approaching, but still lower than the spallation threshold of Ti [20], can be attributed to incomplete periodical spallation, previously observed for Si [23] and Al [24].

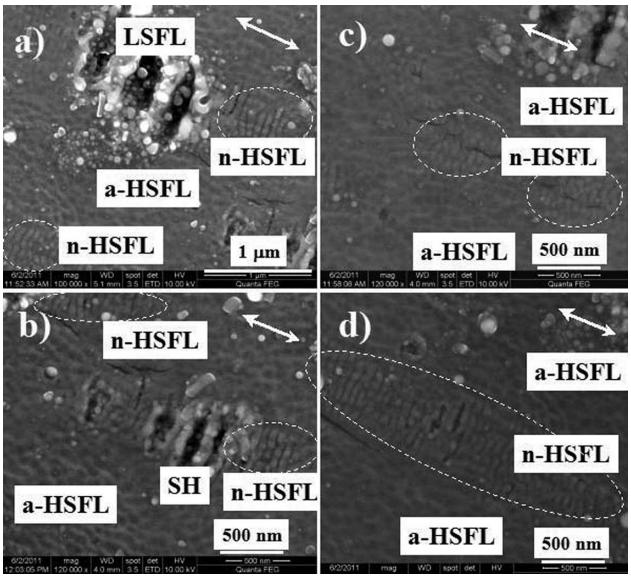

Fig. 1. SEM images of irregular normal (n-HSFLs, shown by the dashed ellipses) and homogeneous abnormal (a-HSFLs) nanoripples with corresponding LSFLs and their second-harmonic (SH) ripples produced across the central part of the focal spot at $F \approx 29$ mJ/cm^2 and $N = 1.5 \times 10^3$. The bilateral arrows show the laser polarization.

To enlighten the underlying electromagnetic picture of such a nanoripple formation, dispersion curves of a Ti surface in air or coated by a thin TiO_2 layer with their dielectric permittivity $\varepsilon_{air} \approx 1 + i0$ and $\varepsilon_{oxide} \approx 7.8 + i(0.04/0.08)$ [10], photoexcited at moderate 744 nm fs-laser fluences F (the absorbed fluence $F_{eff} \approx 0.7F$), were calculated. In these calculations, full equations [25] for K_{SPP}- and K_z-components in the photoexcited metal, air, and oxide were used to describe the SPR region with the resonance condition $\Re e(\varepsilon_m) \approx -\Re e(\varepsilon_d)$, which is beyond the commonly used approximation $\Re e(\varepsilon_m) \ll -\Re e(\varepsilon_d)$, $|\Re e(\varepsilon_m)| \gg \Im m(\varepsilon_m)$ [22]. In particular, K_{SPP}- and K_z-components in the metal ($K_{z,m}$) and dielectric ($K_{z,d}$) media were calculated for $\varepsilon_m = \varepsilon_1 + i\varepsilon_2$ and $\varepsilon_d = \eta_1 + i\eta_2$, respectively, as follows [25]:

$$K_{SPP} = \frac{1}{\lambda}\sqrt{(1/2D)\left[A + \sqrt{A^2 + B^2}\right]}, \tag{2}$$

$$K_{z,m} = \frac{1}{\lambda}\sqrt{\frac{-(\varepsilon_1^2 - \varepsilon_2^2)(\varepsilon_1 + \eta_1) - 2\varepsilon_1\varepsilon_2(\varepsilon_2 + \eta_2) + (\varepsilon_1^2 + \varepsilon_2^2)\sqrt{D}}{2D}}, \tag{3}$$

$$K_{z,d} = \frac{1}{\lambda}\sqrt{\frac{-(\eta_1^2 - \eta_2^2)(\varepsilon_1 + \eta_1) - 2\eta_1\eta_2(\varepsilon_2 + \eta_2) + (\eta_1^2 + \eta_2^2)\sqrt{D}}{2D}}, \tag{4}$$

with the factors A, B, and D defined as [25]

$$\begin{aligned} A &= \eta_1(\varepsilon_1^2 + \varepsilon_2^2) + \varepsilon_1(\eta_1^2 + \eta_2^2), \\ B &= \eta_2(\varepsilon_1^2 + \varepsilon_2^2) + \varepsilon_2(\eta_1^2 + \eta_2^2), \\ D &= (\eta_1 + \varepsilon_1)^2 + (\eta_2 + \varepsilon_2)^2. \end{aligned} \tag{5}$$

In these calculations, we used the previously developed fs-laser photoexcitation model for Ti [8], accounting for the eventual fluence-dependent bleaching of predominating interband transitions from high-density d-bands to low-density s-band due to band filling, and simultaneous rise of interband transitions owing to the larger population of the s-band. Hence, real and imaginary parts of the interband component, $\Re e(\varepsilon_{m,\text{inter}})$ and $\Im m(\varepsilon_{m,\text{inter}})$, of the prompt dielectric function ε_m of the photoexcited Ti increase and decrease to zero, respectively, in contrast to corresponding real and imaginary parts of the intraband component, $\Re e(\varepsilon_{m,\text{intra}})$ and $\Im m(\varepsilon_{m,\text{intra}})$, with the overall $\Re e(\varepsilon_m)$ and $\Im m(\varepsilon_m)$ magnitudes decreasing and increasing, respectively, in the range $F_{eff} < 50$ mJ/cm^2 (Fig. 2) [8]. This ultrafast optical tuning makes the initial broad and weak UV-range SPR at 6.4 eV in air (curve 1 in Fig. 3) monotonously redshifted due to the depleted d-band electron density until 4.1 eV at $F_{eff} \approx 18$ mJ/cm^2 ($\rho \approx 2.5 \times 10^{22}$ cm^3) and

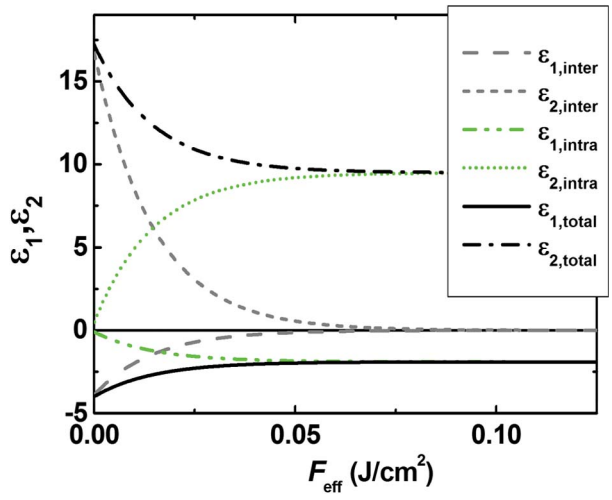

Fig. 2. Fluence dependences of real (solid curves) and imaginary (dashed curves) parts of the dielectric function of Ti, where their interband and intraband components, as well as the overall magnitudes, are shown in gray, green, and black.

4.2 eV at $F_{\text{eff}} \approx 40$ mJ/cm^2 ($\rho \approx 3.6 \times 10^{22}$ cm^3) [curves 2 and 3 in Fig. 3, respectively], while becoming more and more pronounced because of the reduced interband losses for the increasing value ρ. The corrresponding positions of the redshifted SPR vary in Fig. 3 from $K_\infty(6.4\text{ eV}) \approx 4.9$ μm^{-1} till $K_\infty(4.2\text{ eV}) \approx 2.8$ μm^{-1}.

Meanwhile, even for an ultrathin adjacent TiO_2 layer, these SPR resonances become much more pronounced and strongly redshifted by the adjacent dielectric medium by the factor [22] of $[(1+\varepsilon_{\text{oxide}})/(1+\varepsilon_{\text{air}})]^{1/2} \approx 2.1$, appearing now at 3.4 eV for unexcited slightly oxidized Ti ($\rho \approx 0$), at 2.4 eV for $F_{\text{eff}} \approx 18$ mJ/cm^2 ($\rho \approx 2.5 \times 10^{22}$ cm^3) and at 2.0 eV for $F_{\text{eff}} \approx 40$ mJ/cm^2 ($\rho \approx 3.6 \times 10^{22}$ cm^3), with the corresponding SPR positions monotonously shifting down from $K_\infty \approx 5.6$ μm^{-1} until ≈3.9 μm^1 (Fig. 3). The reason is that a thin (typically, a few nanometers thick) natural titanium oxide layer

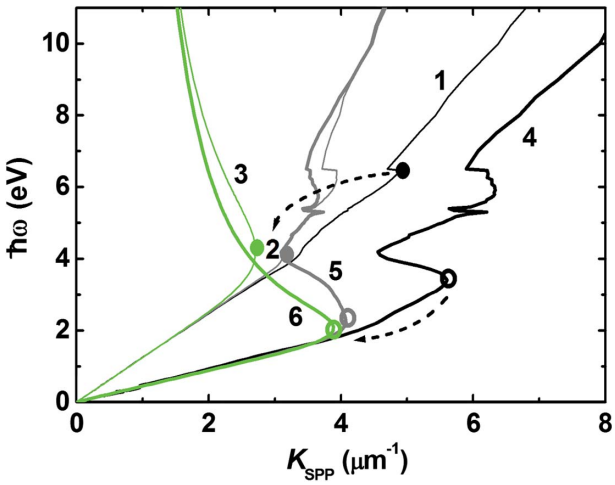

Fig. 3. SPP dispersion curves for Ti/air (thin lines) and Ti/TiO_2 (thick lines) interfaces, calculated for unexcited Ti (curves 1 and 4, black), Ti excited at $F_{\text{eff}} \approx 18$ (curves 2 and 5, gray), and 40 mJ/cm^2 (curves 3 and 6, green), relevant for n- and a-HSFL formations, with the arrows showing their fluence-dependent spectral SPR tuning.

simultaneously works as a bulk oxide medium for longitudinal surface plasmons, which are strongly localized at the surface for the high calculated $K_{z,d} \sim 10$ μm^{-1} [see Eqs. (3) and (4)], while it appears negligible ($\ll\lambda$) for the presumably transverse surface polaritons for the rather low calculated $K_{z,d} \sim 1$ μm^{-1}. (In both of these cases, $K_{z,m} \sim 10$ μm^{-1}) As a result, possible constructive interference of photoexcited counterpropagating short-wavelength surface plasmons can double the wavenumber of the resulting surface interference pattern [9] up to ≈12 μm^{-1} in the UV range and until ≈8 μm^{-1} in the visible range, in contrast with the experimentally observed maximal wavenumbers $1/\Lambda_{a,nH}(744\text{ nm}) \approx 15$–$17$ μm^{-1} (for the minimal periods $\Lambda_{a,nH}(744\text{ nm}) \approx 0.06$–$0.08$ μm) of the even IR (1.67-eV) fs-laser generated surface nanoripples (Fig. 1) (see also [18–20]). Likewise, according to our simulations at lower effective fluences ≤40 mJ/cm^2, the 744 nm laser wavelength always corresponds to an excitation at the air/Ti interface of the only near-wavelength surface polaritons with $K_{\text{SPP}} \approx 1.4$ μm^{-1} (Fig. 3), which are not consistent with the minimal LSFL periods $\Lambda_L(744\text{ nm}) \approx 0.4$ μm in Fig. 1.

To achieve better simulation of the experimental findings, an additional physical effect, which has never been considered, was invoked to modeling. Specifically, extraordinary transient optical states of the photoexcited Ti surface were recently achieved during its ultrafast low-fluence plasma-assisted ablation [26], proceeding via consequent processes of electron emission, reduction of electron density, and surface charging, resulting finally in lifting off electron-ion double-layer plasma plume, as shown for different metals and semiconductors [26,27]. In this case, owing to strong depletion of s- and d-electron density on the metal surface, its plasma frequency Ω_{pl} drops toward, or even below, the optical fs-laser frequency Ω_{las}, while its reciprocal quantity—electron scattering time τ_e—increases somewhat weaker due to the strongly increased electron temperature (~3 eV) [27]. Overall, this may result in some unusual states of electron gas, which are yet to be explored and understood.

Here, a few model regimes (Fig. 4) were considered to simulate ultrafast optical properties of such hot, electron-depleted states with bleached interband transitions of d-electrons as a combination of the above-mentioned prompt optics of the photoexcited oxidized Ti surface and its charging. The regime I with completely bleached interband transitions ($\Re e(\varepsilon_{m,\text{inter}})$, $\Im\text{m}(\varepsilon_{m,\text{inter}}) = 0$) and no charging included shows normal dispersion curves with their 2-eV SPRs, shifting in the range of 3–4 μm^{-1} at increasing F_{eff} (curves 2 and 5 in Fig. 4).

In contrast, the regime II with interband transitions partially present at $F_{\text{eff}} \approx 18$ mJ/cm^2 and bleached at $F_{\text{eff}} \approx 40$ mJ/cm^2 but, with $\Im\text{m}(\varepsilon_{m,\text{intra}}) = 0$, demonstrates sharp IR-range SPRs with corresponding $K_\infty \approx 3$ μm^{-1} and ≈8 μm^{-1} (curves 3 and 6, Fig. 4), respectively. Then, the regime III with the absent Drude contribution ($\Re e(\varepsilon_{m,\text{intra}})$, $\Im\text{m}(\varepsilon_{m,\text{intra}}) = 0$) exhibits no prominent SPR at $F_{\text{eff}} \approx 18$ mJ/cm^2 (curve 4, Fig. 4) while, at $F_{\text{eff}} \approx 40$ mJ/cm^2 ε_m becomes equal to 0 (unphysical case). Hence, more realistic physical representation of the prompt hot and charged Ti surface state with surface nanoripples (wavenumbers $1/\Lambda_{a,nH}(744\text{ nm}) \approx 15$–$17$ μm^{-1}) is obtained in the regime II at $F_{\text{eff}} \approx 40$ mJ/cm^2 ($2K_\infty \approx 16$ μm^{-1}, Fig. 4), assuming complete damping of free-electron absorption at $\Im\text{m}(\varepsilon_{m,\text{intra}}) = 0$.

Finally, the experimentally observed nanoripple polarization flip, from n-HSFL to a-HSFL, in the narrow fluence range

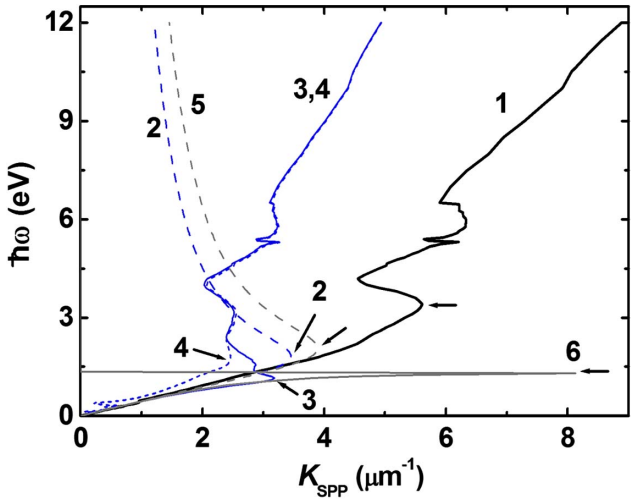

Fig. 4. SPP dispersion curves for Ti/TiO_2 interfaces, calculated for unexcited Ti (curve 1) and Ti photoexcited at $F_{eff} \approx 18$ (curve 2, regime I ; curve 3, regime II ; curve 4, regime III) and 40 mJ/cm^2 (curve 5, regime I ; curve 6, regime II), with the short arrows showing their corresponding SPR positions.

$F \approx 30$ mJ/cm^2 was considered in relation to the fluence-selective SPR excitation on a Ti surface, where its ENZ state appears for $\Re e(\varepsilon_m) \geq -\Re e(\varepsilon_d)$. Such an EM-wave polarization flip for $|\Re e(\varepsilon_m)| \leq \Re e(\varepsilon_d)$ is well known [28], resulting in excitation of a *long-wavelength* surface electromagnetic TM-wave and *microscale* laser-induced periodical surface structures [28]. However, generally such a surface TM-wave can persist not only for $\Re e(\varepsilon_m) \leq -\Re e(\varepsilon_d)$ (the common conditions for SPP existence [21,28]), but also for $|\Re e(\varepsilon_m)| \leq \Re e(\varepsilon_d)$ on a blue SPR shoulder because of SPR broadening for non-negligible $\Im m(\varepsilon_m)$ [see Eqs. (2) and (5) above], with the latter shoulder corresponding to ENZ conditions. Moreover, besides the demonstrated fundamental optical-range dynamic polarization flip of surface plasmons in ENZ states of photoexcited material surfaces, such sub-100-nanometer fs-laser fabricated surface nanoripples may be practically promising large-scale, readily available and somewhat tunable [21] functional elements for sub-100-nanometer EUV optics, surface wetting/freezing and boiling control over the characteristic vapor bubble nucleation scales of ~10–100 nm [29,30]. Transient surface gratings of ε_m with sub-100-nanometer periods can also work as optically switchable, and, potentially, tunable EUV diffraction gratings.

In conclusion, experimentally observed dynamic polarization flip-off for surface nanoripples on a Ti surface, photoexcited by linearly polarized ultrashort laser pulses in the narrow fluence range, was related, through our modeling of its electromagnetic dispersion curves, to different polarizations of surface plasmons on different shoulders of the surface plasmon resonance under ENZ-conditions. Such conditions appear during transient fs-laser photo-excitation and charging of Ti surfaces.

Funding. Österreichische Forschungsförderungsgesellschaft (Austrian Research Promotion Agency) (834325); Government of the Russian Federation (ITMO Visiting Professorship Program) (074-U01).

REFERENCES

1. A. A. Basharin, C. Mavidis, M. Kafesaki, E. N. Economou, and C. M. Soukoulis, Phys. Rev. B **87**, 155130 (2013).
2. T. Wang, J. Luo, L. Gao, P. Xu, and Y. Lai, J. Opt. Soc. Am. B **30**, 1878 (2013).
3. P. Ginzburg, F. J. Rodríguez Fortuño, G. A. Wurtz, W. Dickson, A. Murphy, F. Morgan, R. J. Pollard, I. Iorsh, A. Atrashchenko, P. A. Belov, Y. S. Kivshar, A. Nevet, G. Ankonina, M. Orenstein, and A. V. Zayats, Opt. Express **21**, 14907 (2013).
4. J. J. Yang, Y. Francescato, S. A. Maier, F. Mao, and M. Huang, Opt. Express **22**, 9107 (2014).
5. J. Luo, W. X. Lu, Z. H. Hang, H. Y. Chen, B. Hou, Y. Lai, and C. T. Chan, Phys. Rev. Lett. **112**, 073903 (2014).
6. J. Luo and Y. Lai, Sci. Rep. **4**, 5875 (2014).
7. P. A. Danilov, A. A. Ionin, S. I. Kudryashov, S. V. Makarov, A. A. Rudenko, P. N. Saltuganov, L. V. Seleznev, V. I. Yurovskikh, D. A. Zayarny, and T. Apostolova, J. Exp. Theor. Phys. **147**, 1098 (2015).
8. E. V. Golosov, A. A. Ionin, Y. R. Kolobov, S. I. Kudryashov, A. E. Ligachev, Y. N. Novoselov, L. V. Seleznev, and D. V. Sinitsyn, J. Exp. Theor. Phys. **113**, 14 (2011).
9. A. A. Ionin, S. I. Kudryashov, S. V. Makarov, A. A. Rudenko, P. N. Saltuganov, L. V. Seleznev, and E. S. Sunchugasheva, Appl. Surf. Sci. **292**, 678 (2014).
10. E. D. Palik, *Handbook of Optical Constants of Solids* (Academic Press, 1998).
11. A. Borowiec and H. K. Hagen, Appl. Phys. Lett. **82**, 4462 (2003).
12. J. Bonse, M. Munz, and H. Sturm, J. Appl. Phys. **97**, 013538 (2005).
13. R. Wagner and J. Gottmann, J. Phys. **59**, 333 (2007).
14. G. Miyaji and K. Miyazaki, Opt. Express **16**, 16265 (2008).
15. M. Huang, F. Zhao, Y. Cheng, N. Xu, and Z. Xu, Opt. Express **16**, 19354 (2008).
16. S. Sakabe, M. Hashida, S. Tokita, S. Namba, and K. Okamuro, Phys. Rev. B **79**, 033409 (2009).
17. E. V. Golosov, A. A. Ionin, Y. R. Kolobov, S. I. Kudryashov, A. E. Ligachev, S. V. Makarov, Y. N. Novoselov, L. V. Seleznev, D. V. Sinitsyn, and A. R. Sharipov, Phys. Rev. B **83**, 115426 (2011).
18. E. V. Golosov, V. I. Emel'yanov, A. A. Ionin, Y. R. Kolobov, S. I. Kudryashov, A. E. Ligachev, Y. N. Novoselov, L. V. Seleznev, and D. V. Sinitsyn, J. Exp. Theor. Phys. Lett. **90**, 107 (2009).
19. J. Bonse, J. Krüger, S. Höhm, and A. Rosenfeld, J. Laser Appl. **24**, 042006 (2012).
20. A. A. Ionin, S. I. Kudryashov, S. V. Makarov, L. V. Seleznev, D. V. Sinitsyn, A. E. Ligachev, E. V. Golosov, and Y. R. Kolobov, Laser Phys. Lett. **10**, 056004 (2013).
21. C. S. R. Nathala, A. Ajami, A. A. Ionin, S. I. Kudryashov, S. V. Makarov, T. Ganz, A. Assion, and W. Husinsky, Opt. Express **23**, 5915 (2015).
22. H. Raether, *Surface Plasmons on Smooth and Rough Surfaces and on Gratings* (Springer, 1988).
23. A. A. Ionin, S. I. Kudryashov, L. V. Seleznev, D. V. Sinitsyn, A. F. Bunkin, V. N. Lednev, and S. M. Pershin, J. Exp. Theor. Phys. **116**, 347 (2013).
24. A. A. Ionin, S. I. Kudryashov, A. E. Ligachev, S. V. Makarov, L. V. Seleznev, and D. V. Sinitsyn, J. Exp. Theor. Phys. Lett. **94**, 266 (2011).
25. R. J. Bell, R. W. Alexander, Jr., W. F. Parks, and G. Kovener, Opt. Commun. **8**, 147 (1973).
26. A. A. Ionin, S. I. Kudryashov, S. V. Makarov, P. N. Saltuganov, L. V. Seleznev, D. V. Sinitsyn, V. N. Lednev, and S. M. Pershin, J. Exp. Theor. Phys. Lett. **101**, 308 (2015).
27. A. A. Ionin, S. I. Kudryashov, S. V. Makarov, L. V. Seleznev, and D. V. Sinitsyn, Appl. Phys. A **117**, 1757 (2014).
28. S. A. Akhmanov, V. I. Emel'yanov, N. I. Koroteev, and V. N. Seminogov, Sov. Phys. Usp. **28**, 1084 (1985).
29. L. B. Boinovich and A. M. Emelyanenko, Russ. Chem. Rev. **77**, 583 (2008).
30. I. U. Vakarelski, N. A. Patankar, J. O. Marston, D. Y. C. Chan, and S. T. Thoroddsen, Nature **489**, 274 (2012).